Icarus 322 (2019) 1–12

Contents lists available at ScienceDirect

Icarus

journal homepage: www.elsevier.com/locate/icarus

Resurfacing asteroids from thermally induced surface degradation

Kevin J. Graves[a], David A. Minton[a,*], Jamie L. Molaro[b], Masatoshi Hirabayashi[c]

[a] Department of Earth, Atmospheric, & Planetary Sciences, Purdue University, 550 Stadium Mall Drive, West Lafayette, IN 47907, USA
[b] Planetary Science Institute, 1700 East Fort Lowell, Suite 106, Tucson, AZ 85719-2395, USA
[c] Department of Aerospace Engineering, Auburn University, Davis Hall, Auburn, AL 36849, USA

ARTICLE INFO

Keywords:
Asteroids
Asteroids
Surfaces
Asteroids
dynamics
Near-Earth objects

ABSTRACT

The spectral slopes of S and Q-type asteroids are altered by the weathering of their surfaces due to solar wind interactions and micrometeorite impacts, as well as any processes that work to remove that weathered material. These processes of space weathering and asteroid resurfacing compete with each other to determine the spectral slope of each asteroid, with space weathering raising the spectral slope and resurfacing lowering it. By considering the distribution of spectral slopes with respect to orbital location and size, we can determine which potential resurfacing processes are the most dominant. In this study, we show that the spectral slopes of S and Q-type Near-Earth Asteroids (NEAs) decrease with decreasing perihelion, but only for perihelia $q \lesssim 0.9$ AU. We then use this distribution of spectral slopes vs. perihelion as a constraint for modeling two proposed resurfacing mechanisms. For both models, we numerically integrate the orbits of NEAs over their lifetimes and track their spectral slopes. First, we model the resurfacing of asteroids due to close encounters with the terrestrial planets and found that no combination of parameters could explain the spectral slope vs. perihelion trend at $q \lesssim 0.9$ AU. We also model the resurfacing of asteroids due to thermally induced surface degradation, by assuming a power law relationship between the resurfacing timescale and the solar distance. For a space weathering timescale of an asteroid on a circular orbit at 1 AU of $\tau_{SW0} \lesssim 5$ Myr, we find a range of resurfacing timescales and power law exponents that generate a spectral slope vs. perihelion distribution consistent with observations. We discuss that previous studies supporting the resurfacing of asteroids due to close encounters could be a result of confounding variables, as the correlation of Q-type asteroids' past orbits with the terrestrial planets are confounded by the higher fraction of Q-type asteroids at low perihelia, which could be created by another mechanism. We also discuss previous studies that qualitatively support the process of thermally induced surface degradation at low perihelia, and conclude that thermal processes are the most consistent explanation for resurfacing of asteroids with low perihelia $q \lesssim 0.9$ AU.

1. Introduction

S-type asteroids and Ordinary Chondrite (OC) meteorites share many spectral features. They both show absorption bands at 1 and 2 μm and exhibit the same general spectral shape (DeMeo et al., 2009). Many S-type asteroids are also mineralogically very similar, if not identical, to OC meteorites (Gaffey, 1993; Reddy et al., 2015; Brunetto et al., 2015). However, the spectra of S-type asteroids and OC meteorites are not identical. S-type asteroids typically have a higher spectral slope in the visible and near-infrared wavelengths, and have shallower absorption band depths compared to OC meteorites (Gaffey, 1976; Bus, 1999; DeMeo et al., 2009). S-type asteroids also typically have lower albedos than OC meteorites (Chapman, 2004).

The alteration of asteroid surfaces due to the space environment, or "space weathering," is the generally accepted mechanism to explain the differences between the spectral and albedo properties of S-type asteroids and OC meteorites (e.g., Chapman, 2004; Brunetto et al., 2015). Space weathering includes processes such as ion irradiation from the solar wind and micrometeorite impacts (Brunetto et al., 2015). Space weathering processes can change the spectrum of an asteroid with an OC composition to that of an S-type asteroid by increasing the spectral slope and decreasing its absorption band depths. These spectral changes have been verified by experiments (Sasaki et al., 2001; Clark et al., 2002; Brunetto and Strazzulla, 2005; Strazzulla et al., 2005; Brunetto et al., 2006b; Loeffler et al., 2009), remote sensing (Vernazza et al., 2009), and a sample return from an S-type asteroid, (25143) Itokawa (Noguchi et al., 2011). Additionally, space weathering can darken the surface of a asteroid with an OC composition, creating the albedo

* Corresponding author.
E-mail addresses: graves24@purdue.edu (K.J. Graves), daminton@purdue.edu (D.A. Minton).

https://doi.org/10.1016/j.icarus.2019.01.003
Received 1 August 2018; Received in revised form 28 November 2018; Accepted 4 January 2019
Available online 08 January 2019
0019-1035/

differences between OC meteorites and S-type asteroids (Brunetto et al., 2015).

The presence of Q-type asteroids, with spectra consistent to those of OC meteorites (Bus, 1999; DeMeo et al., 2009), suggests that space weathering has not affected the surfaces of these asteroids. Most of these asteroids have been found in the Near Earth Asteroid (NEA) population and are relatively small ($\lesssim$ 5 km) (Binzel et al., 2004; DeMeo et al., 2014). The best explanation for the presence of Q-type asteroids is that they have recently been resurfaced and have not yet had time for space weathering to create any alteration of their surface. An asteroid is resurfaced if the upper veneer of material that can be altered by space weathering agents (on the order of 10 nm; Noguchi et al., 2011) is removed or buried by unweathered material.

1.1. Space weathering and resurfacing mechanisms

The presence and distribution of Q-type asteroids and less weathered S-type asteroids suggests that there is an ongoing cycle of space weathering and resurfacing. By constraining the timescale of the rate of spectral (or albedo) change from space weathering and the timescale of any potential mechanisms that could resurface asteroids, we can discover which potential resurfacing mechanisms are prevalent.

Laboratory studies and observations of young asteroid families have found space weathering timescales of $\sim$ 10 kyr–1 Myr, if space weathering is controlled by irradiation from the solar wind (Hapke, 2001; Brunetto and Strazzulla, 2005; Strazzulla et al., 2005; Brunetto et al., 2006b; Loeffler et al., 2009; Vernazza et al., 2009) and $\sim$ 100 Myr if space weathering is controlled by micrometeorite impacts (Sasaki et al., 2001; Brunetto et al., 2006a).

Due to the much shorter space weathering timescales derived from the solar wind irradiation, the consensus from these studies is that, for relatively unweathered asteroids, the process of space weathering is dominated by solar wind irradiation (Marchi et al., 2006b; Vernazza et al., 2009; Brunetto et al., 2015).

A space weathering timescale of $\sim$10 kyr–1 Myr places an important constraint on viable resurfacing mechanisms. It implies that disruptive collisions cannot be the primary resurfacing mechanism for creating Q-type asteroids because they occur far too infrequently ($\sim$100 Myr; Bottke et al., 2002; Nesvorný et al., 2005). Nesvorný et al. (2005) proposed that asteroids could instead be resurfaced from the movement of surface grains due to tidal forces during a close encounter with a terrestrial planet, and many additional studies further explored this mechanism (Marchi et al., 2006a; Binzel et al., 2010; Nesvorný et al., 2010; DeMeo et al., 2014; Carry et al., 2016). Nesvorný et al. (2010) found that if a close encounter with a distance of 5 planetary radii is sufficient to cause a complete resurfacing of an asteroid, then resurfacing from close encounters could generate the number of Q-type asteroids in the NEA region for a space weathering timescale of 1 Myr.

Smaller, non-disruptive, collisions can also work to resurface asteroids. The physical excavation and depositing of ejecta, known as impact gardening, will expose unweathered material, lowering the entire spectral slope of the asteroid (Paolicchi et al., 2009; Marchi et al., 2012). Additionally, post-impact seismic shaking could cause overturn or mass movement on an asteroid's surface, especially at high-slope regions, and also expose unweathered material (Richardson et al., 2005; Rivkin et al., 2011; Shestopalov et al., 2013). Both of these processes are difficult to model quantitatively because they are strongly dependent on the spin condition, shape, density, and grain size distribution of the asteroid. For example, see Section 3 in Marchi et al. (2012) for a discussion of the uncertainties in modeling impact gardening. However, Rivkin et al. (2011) used order-of-magnitude arguments to suggest that post-impact seismic shaking is consistent with the existence and distribution of less weathered asteroids found in the Koronis family for a space weathering timescale of $\sim$1 Myr.

The increase in spin rate of an irregularly shaped asteroid due to irregular radiative torques, known as the Yarkovsky-O'Keefe-Radzievskii-Paddack (YORP) effect, can increase an asteroid's spin rate to the point where it fissions or experiences surface or internal failure (Bottke et al., 2006; Walsh et al., 2008; Hirabayashi, 2015). Graves et al. (2018) found that resurfacing from YORP-driven spin-up and failure could explain the number and distribution of less weathered asteroids in the Flora family for a space weathering timescale of 19–80 Myr. However, this timescale is calculated at a solar distance of 2.2 AU, while many of the laboratory-derived timescales are calculated for a near-Earth environment (Brunetto and Strazzulla, 2005; Strazzulla et al., 2005; Loeffler et al., 2009). At 1 AU, their timescales are 4–16 Myr, closer to the range of laboratory-derived timescales.

Finally, thermal cycling and fatigue could cause breakdown of the surface of an asteroid and remove, destroy, or cover any space weathered particles (Delbo et al., 2014). However, the timescale to resurface an asteroid from thermal processes is not well constrained. In summary, the resurfacing mechanisms of close encounters with the terrestrial planets, collisions and subsequent seismic shaking, and YORP-driven spin-up and failure can all potentially resurface asteroids at a rate that can match the number of observed unweathered asteroids for a space weathering timescale of $\sim$10 kyr–1 Myr.

With so many potential mechanisms that could resurface asteroids, additional observational constraints, besides the overall fraction of unweathered to weathered asteroids, are required to determine which mechanisms are the most dominant. A powerful dataset that can help determine the dominant resurfacing mechanisms is the orbital, size, and spectral slope distribution of S and Q-type asteroids. The spectral slope of an asteroid with a OC composition is heavily dependent on the amount of space weathering it has received (Brunetto et al., 2006b). By considering the spectral slope, instead of a binary classification of S vs. Q-type asteroids, we gain information about the degree of weathering. An example of why it is important to consider the degree of weathering can be seen from the results of Mothé-Diniz et al. (2010). They found that the spectra of a subset of S-type asteroids match the spectra of OC meteorites, suggesting that there are S-type asteroids that are relatively unweathered. However, the asteroids that they considered have lower spectral slopes than the majority of S-type asteroids. A binary classification would incorrectly mark these asteroids as completely weathered, but by considering the spectral slope we can more accurately represent the weathering state of these asteroids.

Different resurfacing mechanisms would create different observable orbital and size trends in the spectral slopes of S and Q-type asteroids. By quantifying those trends, we can test the effectiveness of potential mechanisms. The distribution of the spectral slopes of S and Q-type asteroids has been shown to have two primary trends: (1) the average spectral slope decreases with decreasing size, and (2) the average spectral slope decreases with decreasing perihelion in the NEA region. Binzel et al. (2004) first showed that smaller S and Q-type NEAs have lower spectral slopes, on average. Thomas et al. (2011) and Thomas et al. (2012) showed that the trend of less weathered asteroids at smaller sizes is also present in the Koronis family members for diameters $\lesssim$5 km, and Graves et al. (2018) showed the same trend can also be found in the Flora family as well as the entire main belt. Marchi et al. (2006a) first showed that S and Q-type NEAs at lower perihelia also have consistently lower spectral slopes. DeMeo et al. (2014) also found a higher percentage of Q-type asteroids at lower perihelion. As Q-type asteroids typically have lower spectral slopes than S-types, their findings correlate with those of Marchi et al. (2006a).

1.2. Resurfacing mechanisms at low perihelion

Due to the prevalence of the trends towards lower spectral slopes at smaller sizes and lower perihelion, any dominant resurfacing mechanism should explain at least one of these two trends. Graves et al. (2018) showed that resurfacing from YORP-driven spin-up and failure could match the trend of decreasing spectral slope with decreasing size, but could not match the trend of decreasing spectral slope with

decreasing perihelion. In this paper, we assume the model of YORP-driven spin-up and failure in Graves et al. (2018) is a sufficient explanation of the spectral slope vs. size trend. We now test if resurfacing from tidal forces during close encounters with the terrestrial planets or from thermally induced surface degradation can sufficiently explain the spectral slope vs. perihelion trend.

For an asteroid to be resurfaced by a close encounter with a planet, the asteroid must pass very close to the planet. The exact closest approach distance needed to cause a resurfacing event is difficult to determine as it depends on the speed of the asteroid with respect to the planet, the rate of rotation, the spin-pole direction compared to the planet-asteroid plane, and the composition and structure of the asteroid's surface (e.g., Richardson, 1998). However, Richardson (1998) showed that at very small distances ($\lesssim$1.5 planetary radii), nearly all encountering asteroids will break apart. It is reasonable to then assume that a slightly more distant encounter could only resurface (and not disrupt) the asteroid. Because most asteroids with low perihelia still have large aphelia, and therefore cross the orbits of all of the terrestrial planets, tidal effects from close encounters with the terrestrial planets could potentially create the decrease in spectral slopes with decreasing perihelion (Marchi et al., 2006a).

The breakdown of boulders and grains due to thermal cycling has been shown to be effective in terrestrial, Martian, and anhydrous environments (e.g., Eppes et al., 2016; Viles et al., 2010; Delbo et al., 2014), and is expected to also occur in vacuum or low pressure environments such as on the surfaces of comets and asteroids (Thirumalai and Demou, 1970; Dombard et al., 2010; Molaro et al., 2015, Molaro et al., 2017; Auger et al., 2018). Additionally, the magnitude of temperature change increases with decreasing perihelion, increasing the rate of thermal fatigue and degradation. This fracture and degradation can expose underlying unweathered material and resurface the asteroid if either the fractured material is removed from the asteroid, or if a significant amount of the surface material is overturned. Although the timescale of thermally induced surface degradation is not well constrained, if it causes resurfacing at moderately low perihelia, it could create the decrease in spectral slopes with decreasing perihelion.

In this study, we test both potential resurfacing mechanisms – close encounters with the terrestrial planets and thermally induced surface degradation – with a similar resurfacing and space weathering model. We measure the effectiveness of both mechanisms by their ability to match the observed spectral slope vs. perihelion distribution.

The paper is organized as follows. First, we show the observed spectral slope vs. perihelion distribution used as a constraint for our models in Section 2. We show that the spectral slope vs. perihelion trend in the NEA region is only found for perihelia $q \lesssim 0.9$ AU. In Section 3, we describe our generic model structure used in testing both resurfacing mechanisms. Both models track NEAs over their lifetime using an N-body integrator and incrementally increase each asteroid's spectral slope due to space weathering from the solar wind. In Section 4, we model asteroid resurfacing due to close encounters with the terrestrial planets. We show that the spectral slope vs. perihelion trend is not well explained by resurfacing from close encounters. In Section 5, we model asteroid resurfacing as a function of solar distance, as would be expected for thermally induced surface degradation. We show that the spectral slope vs. perihelion trend is well explained by solar distance-dependent resurfacing, and propose that thermally induced surface degradation may better explain the spectral slopes of S and Q-type NEAs than tidally induced resurfacing from close encounters. We discuss our results in Section 6.

2. Distribution of spectral slopes and perihelion

In order to properly test potential resurfacing mechanisms, we must first understand the distribution of spectral slopes at low perihelion. In Fig. 1, we plot the NEA and MC spectral slopes against perihelion, similarly to Fig. (1) in Marchi et al. (2006a). The size of each circle corresponds to the asteroid's diameter, assuming a constant albedo for all asteroids. We also include a windowed moving average of the spectral slopes, where each point is calculated by taking the average of all spectral slopes of asteroids with perihelia that are within ± 0.1 AU. We use a windowed moving average instead of a point-based moving average to better represent the dependence of the asteroids' spectral slopes on perihelion. A point-based moving average will have varying perihelion windows based on the number of observations at different perihelia (e.g., larger windows at low perihelion where less asteroids are observed). The shaded region is the uncertainty of the average spectral slopes at a 95% confidence level. Overall, the average spectral slope decreases with decreasing perihelion from the MCs through the NEAs. However, we find that the average spectral slope only has a significant trend with perihelia for $q \lesssim 0.9$ AU and $q \gtrsim 1.3$ AU, with the slope of the linear regression through the spectral slopes of asteroids with $0.9\text{ AU} \leq q < 1.3$ AU of 0.01 ± 0.26%/μ m/AU.

The trend in the average spectral slope of asteroids with $q \gtrsim 1.3$ AU is most likely due to an observational bias. Since larger S and Q-type asteroids have higher average spectral slopes (Binzel et al., 2004), the larger sizes of the MCs will raise the average spectral slope. Due to this potential observational bias, we restrict our analysis to the NEAs. We include a gray vertical line at $q = 1.2$ AU, above which the running mean is affected by the spectral slopes of MCs. By only considering the NEAs, a resurfacing mechanism only needs to affect asteroids with $q \lesssim 0.9$ AU to match the spectral slope vs. perihelion distribution.

In the remainder of this study, we use the windowed moving average through the observed spectral slope vs. perihelion distribution of the NEAs as our primary constraint on possible resurfacing mechanisms. We also compare the slope of the linear regression through the spectral slopes of asteroids with $q < 0.9$ AU which is 0.52 ± 0.22%/μ m/AU. We use the average spectral slope of all NEAs with $q \geq 0.9$ AU to define the maximum weathering state for our modeled asteroids. In the next section, we build a generic model to estimate the spectral slope vs. perihelion distribution of asteroids due to either resurfacing from tidal effects during close encounters with the terrestrial planets or resurfacing from thermally induced surface degradation.

3. Modeling methods

To model the spectral slopes of asteroids throughout their lifetime in the NEA region, we integrate asteroids from their source regions in the main belt using the regions as defined in Bottke et al. (2002). By starting the asteroids from their source regions and tracking them throughout their entire lifetimes, we record any close encounters with the terrestrial planets, and calculate the integrated amount of space weathering and thermally induced degradation. By combining information on the amount of accumulated space weathering, resurfacing processes, and the current perihelion of each asteroid throughout the simulation, we model the spectral slope vs. perihelion distribution.

In the model of Bottke et al. (2002), the three primary source regions of S and Q-type NEAs are the 3:1 mean motion resonance with Jupiter, the ν_6 secular resonance, and the Intermediate source Mars Crossers (IMCs). The IMCs are a subset of the Mars crossing population that are below the ν_6 resonance and are not in the 3:1 mean motion resonance. We do not consider other source regions, such as the outer belt resonances, because they do not contain a significant number of S and Q-type asteroids (DeMeo and Carry, 2013), and they contribute less to the steady state population of NEAs when compared to the above three (Bottke et al., 2002). We note that there is a recent updated estimate to the near-Earth Object fluxes in Granvik et al. (2018). However, we do not expect our results to significantly change with the inclusion of this updated model because the results of the two resurfacing methods are similar when considering each of the three source regions alone. It appears that, in our model, the estimate of the NEA fluxes plays a minor role compared to the weathering and resurfacing that occurs once the asteroids are in the NEA region.

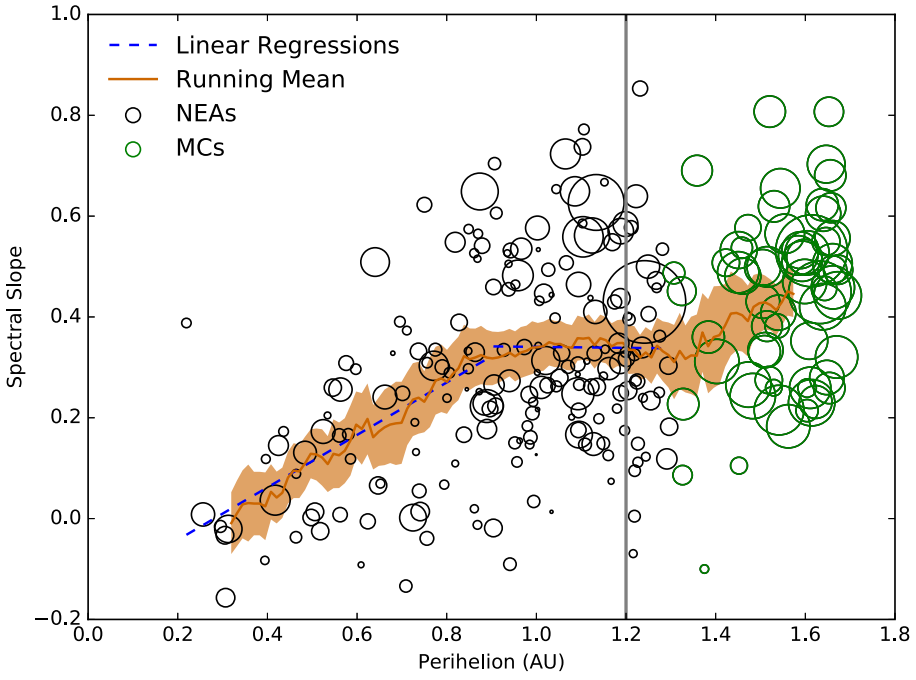

Fig. 1. The distribution of spectral slope vs. perihelion of S and Q-type asteroids in the NEA and MC regions using the data in Binzel et al. (2004) and Lazzarin et al. (2004, 2005). NEAs are drawn as black circles and MCs as green circles. The size of the circle corresponds to the diameter of the asteroid. The dashed blue lines are the linear regressions through the NEA spectral slopes, split at a perihelion of $q = 0.9$ AU. The solid orange line and shaded region is a windowed moving average, where each point is calculated by taking the average of all spectral slopes of asteroids with perihelion that are within ± 0.1 AU, and its uncertainty at a 95% confidence level. This figure is very similar to Fig. 1 from Marchi et al. (2006a), except that we use a windowed moving average instead of a point-based moving average. We denote the perihelion above which MCs affect the windowed moving average by a vertical gray line. The average spectral slope in the NEA region only decreases with decreasing perihelion for $q \lesssim 0.9$ AU. (For interpretation of the references to color in this figure legend, the reader is referred to the web version of this article.)

We integrate the orbits of 6000 asteroids, with 2000 initially in each of our source regions. Asteroids in the 3:1 mean motion resonance with Jupiter are randomly distributed within a semi-major axis of $a = [2.48–2.52]$ AU, an eccentricity of $e < 0.35$, and an inclination of $i < 15$ °. Asteroids in the ν_6 secular resonance begin with a semi-major axis of $a = [2.06–2.37]$ AU, an eccentricity of $e = 0.1$, and an inclination of $i = [2.5–15]$°. The semi-major axis and inclination are selected such that the asteroids fall within the strong part of the ν_6 resonance, described in detail in Morbidelli and Gladman (1998). Asteroids in the IMCs are generated to match the semi-major axis, inclination, and eccentricity distribution of observed asteroids with a magnitude of $H < 16$ in the IMC region, using 3373 asteroids pulled from the JPL Small Body Database (ssd.jpl.nasa.gov). These initial conditions are very similar to those in Bottke et al. (2002), and generate statistically similar NEAs.

We use a Regularized Mixed Variable Symplectic (RMVS) integrator in the SWIFTER N-body code (Levison and Duncan, 1994) to integrate the asteroids. We include all eight major planets, but do not account for the general relativistic effects on Mercury's orbit. We integrate all asteroids with a 1 day timestep and the simulation runs for 100 Myr. We tested a subset of our model with a 12 hour timestep and found no difference in the final average spectral slope vs. perihelion distribution. We also remove asteroids from the simulation if they collide with the Sun or a planet or have a semi-major axis larger than 1000 AU. Due to the relatively short integration time of 100 Myr and the chaotic nature of NEAs, we do not expect the small deviations in Mercury's orbit from general relativistic effects to change the close encounter statistics or the orbital distributions of the NEAs. Additionally, encounters with Mercury are very rare compared to encounters with the other terrestrial planets. The integrator records all close encounters between asteroids and planets within 3.5 Hill Radii of the planet.

We also simulate the increase in the asteroids' spectral slopes over time using a simplified space weathering model. If an asteroid remains in its current orbit and experiences no resurfacing events, the rate of change of the spectral slope depends on the current spectral slope of the asteroid (Brunetto et al., 2006b; Willman et al., 2010; Graves et al., 2018). In other words, the spectral slope of an asteroid being space weathered follows an exponential saturation curve, where the rate of increase of its spectral slope decreases as the asteroid becomes more weathered. Since we constrain the spectral slope to a maximum value of S_{max}, we can express the rate of change in spectral slope due to space weathering as:

$$\left(\frac{dS}{dt}\right)_{SW} = \frac{1}{\tau_{SW}}(S_{max} - S). \tag{1}$$

where S is the slope of the asteroid and τ_{SW} is its e-folding space weathering timescale.

We assume that the process of space weathering is dominated by the alteration of an asteroid's surface by the solar wind because of its much shorter timescale. Because the intensity of the solar wind scales with the solar distance as $1/r^2$, we scale the space weathering timescale accordingly:

$$\tau_{SW} = \frac{\tau_{SW0}}{(1\text{ AU})^2}\frac{P}{\oint r^{-2}dt} = \frac{\tau_0}{(1\text{ AU})^2}a^2\sqrt{1-e^2}, \tag{2}$$

where r is the instantaneous solar distance of the asteroid, P is the orbital period, a and e are its semi-major axis and eccentricity, and τ_{SW0} is the space weathering timescale at $a = 1$ AU and $e = 0$. The integral in Eq. (2) is taken over one orbit. Throughout the simulation, the asteroid's orbit evolves, and the space weathering timescale τ_{SW} changes. Thus, we increment the spectral slope at each timestep with Eq. (1) to accurately represent the spectral slope over its evolution throughout the NEA region.

We select the minimum spectral slope, S_{OC}, and maximum spectral slope, S_{max}, for each asteroid randomly from Gaussian distributions. We use the spectral slopes of OC meteorites to calculate the value of S_{OC}, with the mean value $\mu_{OC} = 0$ and the standard deviation $\sigma_{OC} = 0.05$, approximately matching the OC spectral slopes used in Vernazza et al. (2009). We use the distribution of spectral slopes from NEAs with perihelia $q > 0.9$ AU to calculate the value of S_{max} (Fig. 1). By using the average spectral slope for NEAs with $q > 0.9$ AU, we are not necessarily finding the average spectral slopes of completely weathered S-type asteroids. There are other resurfacing mechanisms that can lower the average spectral slope of the entire population, but there is no significant spectral slope vs. perihelion trend at $q > 0.9$ AU. We find a mean value of $\mu_{max} = 0.34$ and standard deviation of $\sigma_{max} = 0.1$.

At the beginning of the simulation, all asteroids start at S_{max}, simulating a lack of spectral slope vs. perihelion trend in the MCs and main belt. Then, throughout the integration, an asteroid can experience resurfacing processes either through close encounters or thermally

induced degradation. These effects, which are described in Sections 4.1 and 5.1, will cause the spectral slopes of asteroids to decrease. We calculate the change in spectral slope on each asteroid from space weathering every 10^4 years. For the close encounter resurfacing model, we apply the change in the spectral slopes due to a resurfacing encounters at the time of the encounter, and for the thermally induced degradation model, we also calculate the change in spectral slope on each asteroid every 10^4 years. We then save the perihelion and spectral slope of each asteroid in the NEA region every 10^5 years throughout the simulation to measure the effect of the resurfacing and weathering processes on the spectral slope vs. perihelion distribution. Shorter timesteps for calculating the change in spectral slope and for saving the perihelion and spectral slope of each asteroid yield similar results.

We use the positions and spectral slopes from timesteps throughout the simulation to generate a representative sample of the steady-state NEA distribution. According to Bottke et al. (2002), the ν_6 resonance, the 3:1 resonance, and the IMCs generate approximately 37%, 27%, and 20% of the population of NEAs at any given time. By simply selecting all asteroids in the NEA region every 10^5 years, we will not generate the appropriate total fraction of asteroids evolving from each source region. To account for the relative flux from each source region, we artificially duplicate instances of a perihelion and a spectral slope of an asteroid at a random time from underrepresented source regions until we find the correct distribution. Specifically, we find the number of saved asteroids from each source region across all timesteps: $N_{3:1}$, N_{ν_6}, and N_{IMC}. Then, we find the maximum of ($N_{\nu_6}/0.37$, $N_{3:1}/0.27$, $N_{IMC}/0.2$) corresponding to the source region that has the largest number of asteroids over the needed fraction. We artificially increase the number of the other two source regions and repeat this process until we reach the appropriate fractions for each source region.

For both resurfacing mechanisms, we consider a range of possible parameters. Due to the computational cost of running the N-body integration, we reuse its results for each set of parameters. For each new parameter set, we select a new S_{max} and S_{OC} for each asteroid from the appropriate distribution, and evolve the spectral slopes according to the model and the specific parameters. There are two primary sources of uncertainty in calculating the windowed moving average from the modeled asteroids: (1) the selection of S_{max} and S_{OC} for each asteroid at the beginning of the simulation, and (2) the randomized artificial increase in the number of asteroids from underrepresented source regions. To reduce the uncertainty from these two sources, we run each set of parameters 12 times with randomized values of S_{max} and S_{OC} and randomized duplication of asteroids from underrepresented source regions for each iteration. The final spectral slope vs. perihelion distribution for a specific set of parameters is the combination of all of the spectral slope and perihelion pairs from all 12 iterations.

After applying these iterations, we have almost 4 million total sets of perihelia and spectral slopes from all iterations (including all source regions) for each set of parameters to compare to the NEA distribution in Fig. 1. We calculate the windowed moving average through the modeled spectral slope vs. perihelion NEA distribution with a window size of ± 0.1 AU. We then calculate the Root Mean Square Error (RMSE) between the windowed moving averages of the observed spectral slope vs. perihelion distribution and the modeled distribution. A lower RMSE corresponds to a better fit, and we define acceptable solutions by the condition that ≥ 95% of the points on the modeled windowed moving average must fall within the 95% confidence intervals of the windowed moving average of the observed NEAs in Fig. 1. Due to the multiple iterations at each set of parameters, the uncertainties of the modeled distributions' windowed moving averages are over an order of magnitude less than those from the observed distribution. Thus, we only consider the uncertainties from the observed distribution. In the next section, we include resurfacing from planetary close encounters in our model, and show the results in Section 4.2.

4. Resurfacing from close encounters

4.1. Methods

To include resurfacing from close encounters, we follow the "NEA model" described in Nesvorný et al. (2010), except that we model the spectral slopes instead of the S vs. Q-type classification. We gather all close encounters in the simulation and select a maximum resurfacing distance, r^*, in planetary radii (R_{pl}) inside which all asteroids will experience a complete resurfacing event. By considering only the maximum resurfacing distance, we simplify the complex behavior of asteroids during close encounters, but we capture the average required resurfacing distance for a population of asteroids. Additionally, by using planetary radii, we approximately scale for tidal gravity between all planets (Richardson, 1998). After an asteroid experiences a resurfacing encounter with a planet, we select its spectral slope from the S_{OC} distribution to estimate an unweathered surface. Then, the asteroid incrementally weathers each time step due to the solar wind using Eq. (1).

We simulate the spectral slopes vs. perihelion distribution for the range of space weathering timescales, τ_{SW0} = 10 kyr–100 Myr, and for maximum resurfacing distances, r^* = 1.5–20 R_{pl}. The range of space weathering timescales encapsulates those estimated through other studies with solar wind as the primary weathering agent (Brunetto et al., 2015). We extend the maximum range of the space weathering timescale to 100 Myr because better solutions were found at long timescales. The upper bound of maximum resurfacing distances of 20 R_{pl}, is distant enough that we should not expect any tidal effects to be relevant at that distance (Richardson, 1998; Walsh and Richardson, 2008).

4.2. Results

We plot the RMSE between the windowed moving averages of our simulated and observed distributions in Fig. 2 for the entire range of tested parameters. No set of parameters produce a windowed moving average that has ≥ 95% of its points within the 95% confidence intervals of the observed distribution in Fig. 1. Also, there are no solutions that can match the steep slope of the linear regression at $q < 0.9$ AU. Thus, no combination of τ_{SW0} and r^* can provide a spectral slope vs. perihelion distribution that resembles the observed NEA distribution.

Fig. 3 shows the windowed moving average through the distribution of spectral slopes vs. perihelia and the linear regression at $q < 0.9$ AU for a simulation with τ_{SW0} = 100 Myr and r^* = 3.4 R_{pl}. This combination of parameters represents the minimum RMSE for all tested parameters, with RMSE = 0.07%/μ m. The windowed moving average has the same window size as the observed moving average of ± 0.1 AU. The uncertainties on the modeled windowed moving average are smaller than the width of the line. We also show the windowed moving average and the linear regression at $q < 0.9$ AU for the observed NEAs reproduced from Fig. 1.

The windowed moving average of the modeled distribution in Fig. 3 is visibly not a good fit for the observed spectral slope vs. perihelion distribution. There are large deviations between the observed and modeled windowed moving averages, especially at low perihelia. Additionally, the slope of the linear regression at $q < 0.9$ AU is 0.170 ± 0.004%/μ m/AU, significantly different than the slope through the linear regression of observed NEAs (0.52 ± 0.21%/μ m/AU).

From these results, we can confidently conclude that resurfacing asteroids from close encounters with the terrestrial planets is not a dominant resurfacing mechanism for S and Q-type NEAs. However, this conclusion is contrary to many previous studies (e.g., Marchi et al., 2006a; Binzel et al., 2010; Nesvorný et al., 2010; DeMeo et al., 2014; Carry et al., 2016). In Section 6.1, we discuss how the correlation between close encounters and Q-type asteroids found in many of these studies is most likely due to confounding variables. In the next section,

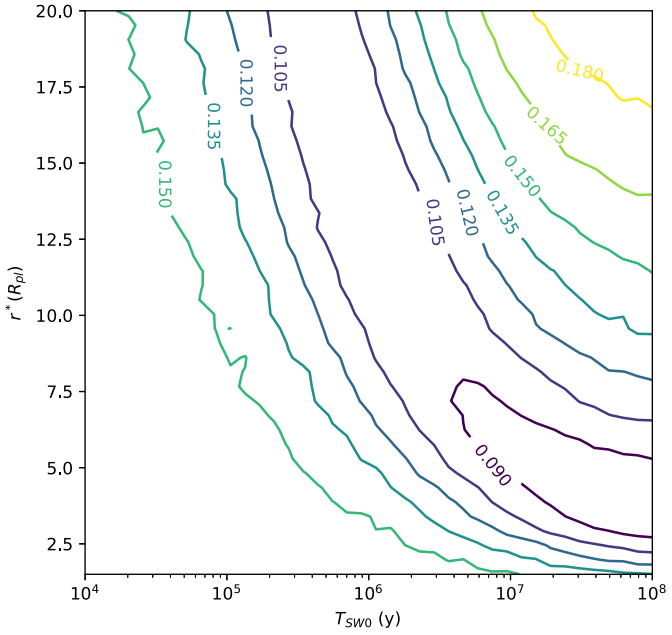

Fig. 2. A contour plot of the Root Mean Square Error (RMSE) between the windowed moving averages of the observed spectral slope vs. perihelion distribution and the modeled spectral slope vs. perihelion distribution generated by resurfacing from close encounters with the terrestrial planets. No combination of the parameters τ_{SW0} and r^* can generate windowed moving averages with > 95% of the points within the 95% confidence intervals of the observed NEA distribution in Fig. 1.

we investigate a model for resurfacing asteroids from thermally induced degradation, and show that it can provide a better fit to the spectral slope vs. perihelion distribution in the NEA region compared to resurfacing from close encounters.

5. Resurfacing from thermally induced surface degradation

5.1. Methods

It has been well established in the engineering literature that the growth rate of macroscopic cracks as a result of thermal fatigue goes as a power law with the induced cyclic stress (e.g., Janssen et al., 2002; Paris and Erdogan, 1963; Le et al., 2014; Ritchie, 2005). Measurements of such power laws are strongly dependent on the material size and shape, the size of the initial crack, and the environment, so they cannot be generalized to the case of asteroid surfaces. However, if we consider that the breakdown of boulders, production of regolith, and exposure of fresh material on these asteroids depends, in part, on the growth of many fatigue cracks in and across the surface, then it is not unreasonable to hypothesize that their convolved effect on the removal of space weathered surface material – or the resurfacing rate – also follows some power law with stress (a similar argument was also made in Marchi et al., 2009). Additionally, the thermally induced stress in an object is directly proportional to the amplitude of its diurnal temperature range (e.g., Molaro et al., 2015). For fast rotating bodies (with periods less than one Earth day), such as most asteroids, the amplitude of its diurnal temperature range is primarily controlled by the solar distance (Marchi et al., 2009; Molaro et al., 2017). Thus, we make the reasonable assumption that the total rate of surface degradation on an asteroid's surface has a power law relationship with the solar distance.

For resurfacing to occur from thermal effects, the thermal cycling would cause cracks to form on the surface boulders of the asteroid, and those growing cracks would eventually break off sections of the boulders' surfaces. Then, any resulting debris or regolith would need to be moved across the surface or completely removed from the asteroid to expose the underlying unweathered material (see Section 6.2 for further discussion). Because space weathering only affects the upper microns of the regolith grains on an asteroid (Noguchi et al., 2011), any location where breakdown and subsequent surface movement or material removal occurs will expose completely unweathered material. Additionally, the bulk spectral slope of an asteroid is a combination of the spectral slopes across all arbitrary subdivisions of the observed hemisphere. Thus, as small sections are resurfaced, the bulk spectral slope of the asteroid is lowered. However, if a highly weathered section is resurfaced, there will be a larger change in the bulk spectral slope than if a

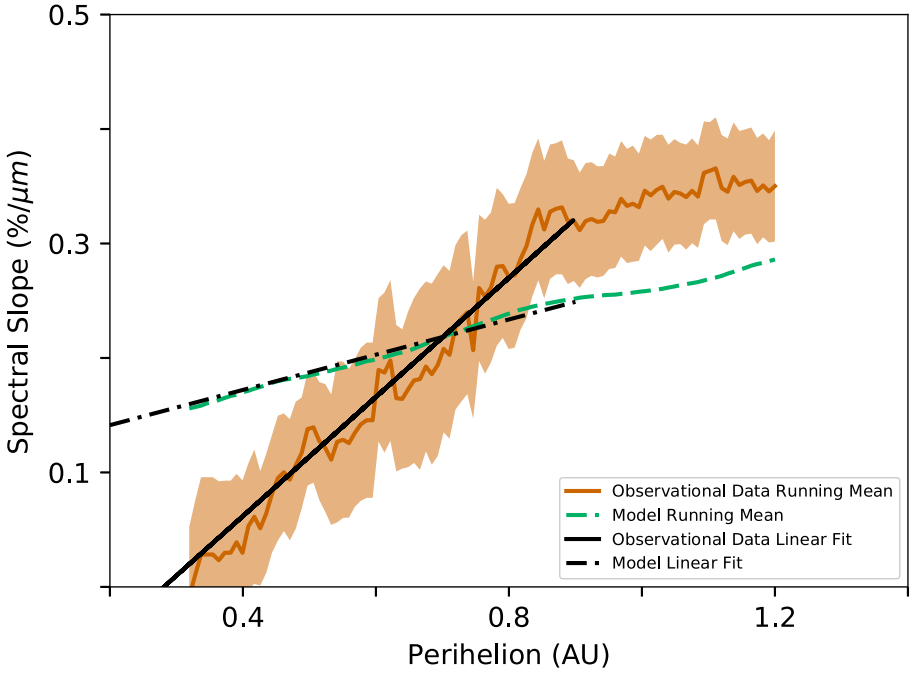

Fig. 3. The windowed moving average and the linear regression at $q < 0.9$ AU of the asteroids' spectral slope vs. perihelion distribution from resurfacing due to close encounters with the terrestrial planets for the best fit solution of $\tau_{SW0} = 100$ Myr and $r^* = 3.4\ R_{pl}$. The dashed green curve is the windowed moving average of the spectral slopes of the modeled asteroids. The uncertainty is smaller than the thickness of the line. The solid orange line is the average observed NEA spectral slopes and the shaded region is its uncertainty at a 95% confidence level (from Fig. 1). Both moving averages have a window size of ± 0.1 AU. Only 42% of the points on the modeled windowed moving average fall within the error bounds of the observed moving average. The dashed-dotted black line and the solid black line are the linear regressions for $q < 0.9$ AU of the modeled and observed asteroids, respectively. For clarity, the error bars for the slopes of the linear regressions are not shown (see Section 4.2 for the errors), but the slope of the modeled asteroids' linear regression does not match the steep slope of the observed linear regression at $q < 0.9$ AU. (For interpretation of the references to color in this figure legend, the reader is referred to the web version of this article.)

relatively unweathered section is resurfaced. Thus, the rate of change of an asteroid's bulk spectral slope from thermally induced resurfacing should approximately depend on the current bulk spectral slope of the asteroid, assuming that the spectral slope doesn't greatly change across the surface of the asteroid.

In our model implementation, we assume that the averaged rate of change in the bulk spectral slope due to the resurfacing of small sections across the body linearly depends on the current bulk spectral slope of the asteroid. Specifically, we calculate the rate of change of the spectral slope as:

$$\left(\frac{dS}{dt}\right)_R = \frac{1}{\tau_R}(S_{OC} - S). \tag{3}$$

where τ_R is the e-folding resurfacing timescale. Eq. (3) satisfies the need for a more rapid rate of decrease in the spectral slope for more highly weathered asteroids. We also found that the exact formulation of the rate of change in the spectral slope due to resurfacing does not greatly alter our results.

We then increment the spectral slope, S, at each time step using Eqs. (1) and (3). Due to our relatively large timestep of 10^4 y, an incremental change in spectral slope can become large when τ_{SW} or τ_R become small. However, for a given τ_{SW} and τ_R, there is a spectral slope (S^*) between S_{OC} and S_{max} where the space weathering and resurfacing rate cancel each other. By setting Eq. (1) equal to the negative of Eq. (3), we find

$$S^* = \frac{\tau_R S_{max} + \tau_{SW} S_{OC}}{\tau_R + \tau_{SW}}. \tag{4}$$

We create a constraint that if an incremental step in spectral slope would cross S^*, then we set $S = S^*$.

Following our argument at the beginning of this section, we let the resurfacing timescale, τ_R, scale with the solar distance, r, raised to some unknown power k:

$$\tau_R = \frac{\tau_{R0}}{(1\ \mathrm{AU})^2}\frac{P}{\oint r^{-k}dt} = \frac{\tau_{R0}}{(1\ \mathrm{AU})^2}\frac{2\pi a^k(1-e^2)^{k-3/2}}{\oint (1+e\cos(f))^{k-2}\,df}, \tag{5}$$

where f is the true anomaly, P is the orbital period, and τ_{R0} is the resurfacing timescale at $a = 1$ AU and $e = 0$. As in Eq. (2), the integral is taken over one orbit. The integral in Eq. (5) cannot be solved analytically in general, but it can be solved numerically and rapidly with the use of Gaussian hypergeometric functions.

Due to the limited constraints on thermally induced surface degradation, we have 3 relatively unconstrained parameters to explore: the space weathering and resurfacing timescales for a circular orbit at 1 AU, τ_{SW0} and τ_{R0} respectively, and the power law exponent controlling the dependence of the resurfacing timescale on solar distance, k. To simplify the parameter space, we searched over 10 logarithmically spaced values of space weathering timescales from $\tau_{SW0} = 10$ kyr–10 Myr, and vary $\tau_{R0}/\tau_{SW0} = 10^{-1}$–$10^8$ and $k = 1.5$–35. We use the parameter τ_{R0}/τ_{SW0} instead of τ_{R0} because comparing the plots with different values of space weathering timescales (τ_{SW0}) is more intuitive.

5.2. Results

Fig. 4, shows three contour maps of the RMSE between the windowed moving averages of the modeled and observed spectral slope vs. perihelion distributions. The top, middle, and bottom plots are calculated with $\tau_{SW0} = 10$ kyr, 100 kyr, and 1 Myr respectively. We also shade acceptable solutions, where ≥ 95% of the points on the windowed moving average of the modeled distribution are within the 95% confidence intervals of the observed distribution. We find a small range of acceptable solutions for $\tau_{SW0} = 10$ kyr with $k \approx 5$–10, and $\tau_{R0}/\tau_{SW0} \approx 2$–50. For $\tau_{SW0} = 100$ kyr and $\tau_{SW0} = 1$ Myr, we find a large range of solutions with $k \gtrsim 6$ and $\tau_{R0}/\tau_{SW0} \gtrsim 5$, with no upper bound in the tested parameter space. Considering all 10 tested values of τ_{SW0}, we find acceptable solutions with $\tau_{SW0} \lesssim 5$ Myr, $k \gtrsim 5$ and $\tau_{R0}/\tau_{SW0} \gtrsim 2$. We choose not to extend the parameter space for k and τ_{R0}/τ_{SW0} because higher values produce increasingly higher RMSEs, and exceedingly high values of k are likely not physical.

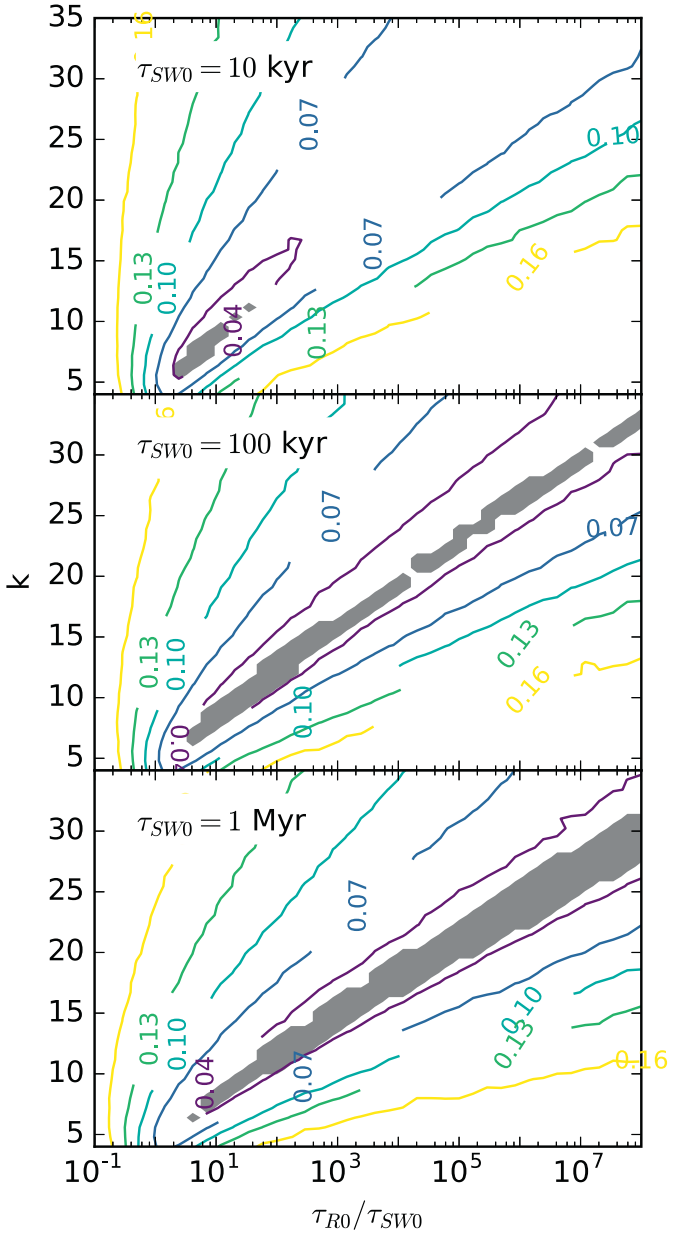

Fig. 4. Three contour plots showing the RMSEs between the windowed moving averages of the spectral slope vs. perihelion distribution from the thermally induced resurfacing model and the observed data. The top, middle, and bottom frames show the RMSEs for the space weathering timescales of $\tau_{SW0} = 10$ kyr, 100 kyr, and 1 Myr respectively. The shaded regions correspond to solutions where ≥ 95% of the points on the modeled windowed moving average fall within the error bounds of the observed moving average. For all tested values of τ_{SW0}, the parameters that provide acceptable solutions are $\tau_{SW0} \lesssim 5$ Myr, $k \gtrsim 5$, and $\tau_{R0}/\tau_{SW0} \gtrsim 2$.

Fig. 5, shows the windowed moving average and the linear regression at $q < 0.9$ AU of the spectral slope vs. perihelion distribution for $\tau_{SW0} = 22$ kyr, $\tau_{R0}/\tau_{SW0} = 7$ ($\tau_{R0} \approx 150$ kyr), and $k = 8$. This combination of parameters represents the minimum RMSE for all tested parameters, with RMSE = 0.018%/μ m. As in the Fig. 3, the windowed moving average has a window size of ± 0.1 AU, and the uncertainty of the modeled distribution is smaller than the thickness of the line. We also show the windowed moving average and the linear regression at

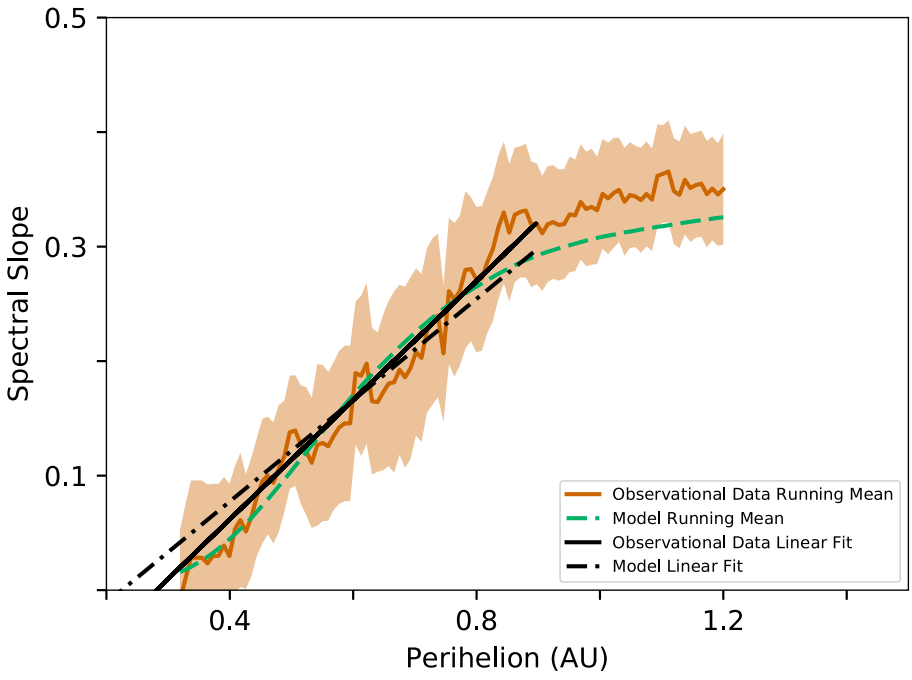

Fig. 5. Identical to Fig. 3 except showing the results from the thermally induced resurfacing model for the parameters: $\tau_{SW0} = 22$ kyr, $\tau_{R0}/\tau_{SW0} = 7$ ($\tau_{R0} \approx 150$ kyr), and $k = 8$. These parameters represent the smallest RMSE between the windowed moving averages of the modeled and observed spectral slope vs. perihelion distributions of NEAs. We found that 98% of the points on the modeled windowed moving average fall within the error bounds of the observed moving average. The slope of the linear regression at $q < 0.9$ AU of the modeled asteroids also falls within the error bounds of slope of the linear regression for the observed data (see Section 5.2 for details). All parameters that fall within the shaded regions of Fig. 4 will generate a similar plot.

$q < 0.9$ AU for the observed NEAs.

The parameters in Fig. 5 provide a very good fit to the spectral slope vs. perihelion distribution. The slope of the linear regression at $q < 0.9$ AU is $0.4656 \pm 0.0005\%/\mu$ m/AU, which is also consistent with the observed distribution of NEAs ($0.52 \pm 0.21\%/\mu$ m/AU). All of the acceptable solutions, which are shaded in Fig. 4, provide similar fits as the one shown in Fig. 5, and are able to match the slope of the linear regressions at $q < 0.9$ AU of the observed distribution of NEAs. When comparing Figs. 5 and 3, resurfacing asteroids from thermally induced surface degradation can provide a much better explanation for the decrease in spectral slopes at low perihelia.

The large region of acceptable solutions supports solar distance dependent resurfacing as a natural explanation for producing the spectral slope vs. perihelion trend. However, a robust and quantitative conclusion for whether resurfacing from thermally induced degradation as a solar distance dependent resurfacing process is occurring on the surface of asteroids, may require precise knowledge of all three parameters — τ_{SW0}, τ_{R0}, and k. This work – specifically Fig. 4 – builds a functional relationship between these three parameters, and future work can help constrain the region of acceptable solutions. We discuss these results and additional qualitative and quantitative evidence for thermally induced surface degradation in Section 6.2.

6. Discussion

By modeling the population of NEAs, we were able to test the effectiveness of resurfacing S and Q-type asteroids from either tidal effects during close encounters with the terrestrial planets or thermally induced degradation at low solar distances. We find that resurfacing from close encounters cannot adequately match the observed spectral slope vs. perihelion distribution, and that a thermally induced degradation process modeled as a solar distance dependent resurfacing model provides a much better fit. In this section we discuss both results. We show how previous studies supporting the close encounter mechanism are most likely confounded by an underlying distribution of less weathered asteroids at low perihelion. We also consider the acceptable solutions of the thermally induced surface degradation models and show that they agree with the process of thermal fracture on the surface of an asteroid.

6.1. Resurfacing from close encounters

Resurfacing asteroids from close encounters with the terrestrial planets cannot generate a spectral slope vs. perihelion distribution that is consistent with the observed distribution. However, previous studies by Binzel et al. (2010) and Carry et al. (2016) used the correlation between Q-type asteroids and recent low Mean Orbital Intersection Distances (MOIDs) and low close encounter distances with the terrestrial planets instead of relying on the spectral slopes. Here, we argue that the correlations in these studies are confounded by the higher fraction of Q-types at low perihelia created by another resurfacing mechanism (such as thermally induced surface degradation).

Binzel et al. (2010) cloned all observed Q and S-type NEAs and MCs, six times and conducted backwards simulations of all asteroids and clones. Over their 0.5 Myr integrations, they selected the lowest MOID from all timesteps for each asteroid and its clones, which we refer to at the minimum MOID. They found that all Q-type asteroids had a minimum MOID within the lunar distance, while this was not true for the S-types. Using binomial statistics, they found a probability of 0.9% that all Q-types would have a minimum MOID within the lunar distance if they were randomly sampled from the distribution of their population of S and Q-type asteroids. Even though Q-type asteroids were later observed in the NEA and MC regions that do not have a minimum MOID within the lunar distance (DeMeo et al., 2014), this statistical argument still suggests a strong correlation between Q-type asteroids and a low minimum MOID with Earth.

Carry et al. (2016) used observations from the Sloan Digital Sky Survey, and conducted similar backwards simulations for NEAs and MCs with about 100 clones for each asteroid. They counted the number of close encounters of each asteroid and all of its clones with Venus, Earth, and Mars. They found that Q-type asteroids have more resurfacing encounters than S-types for Venus and Earth, but no difference between S-types and Q-types for encounters with Mars. They did not attempt to correlate each Q-type asteroid to a recent resurfacing event with a terrestrial planet, but they did conclude that Q and S-type asteroids are dynamically different and that Q-types tend to have more close encounters with Earth and Venus.

Using the data from the supplementary material of Binzel et al. (2010), we found that 100% of all asteroids with $q < 0.9$ AU have a minimum MOID within the lunar distance of Earth, including 13 Q-type

asteroids. Therefore, there is no significance that the Q-types at $q < 0.9$ AU have low minimum MOIDs because all asteroids in their study at $q < 0.9$ AU have low minimum MOIDs. If we remove these asteroids due to their lack of significance, and also remove the MCs from the calculation because they are unable to have low MOIDs with Earth, we find that the fraction of asteroids with $0.9 < q < 1.3$ AU with low minimum MOIDs is 30/42. The probability that all 7 Q-types with $0.9 < q < 1.3$ AU have a minimum MOID within the lunar distance if they are randomly sampled is $(30/42)^7 \approx 9\%$, much less significant than 0.9%.

Additionally, the conclusion that Q-types tend to have more close encounters with Earth and Venus, on average, from Carry et al. (2016) is certainly correct. However, it is difficult to gain any insight into whether close encounters have actually resurfaced these Q-types unless we consider similar populations of S and Q-type asteroids. The majority of asteroids that Carry et al. (2016) considered for close encounters with Earth and Venus were MCs, and the majority of MCs that they observed are S-types. Q-type asteroids only comprised a significant fraction of their population for the NEAs. By including MCs that are heavily weighted towards S-types and that cannot have close encounters with Earth or Venus, the cumulative number of close encounters of S-type asteroids with Earth and Venus will naturally grow more slowly than Q-types, even if both S and Q-type NEAs have the same average number of close encounters. If the MCs were removed from the analysis, it is unclear if the remaining Q-types NEAs would have more close encounters with Earth and Venus than compared to S-type NEAs, and the significance of their results would certainly decrease.

Furthermore, Nesvorný et al. (2010) found that resurfacing from close encounters with the terrestrial planets could explain the overall number of Q-types in the NEA population but could not match their orbital distribution. They noticed a bimodal distribution of Q-type asteroids at semi-major axes $a \lesssim 1$ AU and $a \gtrsim 1.5$ AU, which has since been smoothed out with more observations (DeMeo et al., 2014). However, they found that they were not able to match both populations simultaneously. In particular, when they used a space weathering timescale that scaled with solar wind irradiation ($1/r^2$), they were unable to match the low a (and low q) population, consistent with our inability to match the very low spectral slopes at low perihelia by resurfacing from close encounters.

We conclude that tidal effects from close encounters with the terrestrial planets are not a dominant resurfacing mechanism for S and Q-type asteroids for the following reasons: (1) close encounters are unable to generate the observed spectral slope vs. perihelion distribution for any reasonable range of space weathering timescales and maximum resurfacing distances, and (2) the previous correlations between Q-type asteroids and low MOIDs or close encounters with the terrestrial planets in backwards simulations can be explained by a larger fraction of Q-type asteroids at low perihelion. It is possible that very close encounters with the terrestrial planets can still resurface some asteroids, but those events do not appear to play a large role in the population of S and Q-type asteroids. In the next subsection, we discuss the results from our thermally induced surface degradation model, which can provide a much more consistent fit to the observed spectral slope vs. perihelion distribution of NEAs.

6.2. Resurfacing from thermally induced surface degradation

In Section 5.1, we cite evidence that suggests the breakdown of the surface of an asteroid due to thermal cycling can be well represented by a power law. However, we did not place any limits on the power law relationship, and allowed both τ_{R0} and k to be unconstrained parameters. From the acceptable solutions of our solar distance dependent resurfacing model, we conclude that the process of thermally induced surface degradation produces a good representation of the observed spectral slope vs. perihelion distribution, only if our acceptable solutions are consistent with the process of thermal fracture. Here, we argue that the range of acceptable solutions are consistent, and that other observations and modeling studies qualitatively support the process of thermal breakdown at low perihelia.

The acceptable values of $\tau_{SW0} \lesssim 5$ Myr generally fit with experimental results. Interestingly, this upper bound is barely consistent with the range of space weathering timescales at $a = 1$ AU and $e = 0$ required for YORP spin-up and failure to be a primary resurfacing mechanism for asteroids at small sizes (Graves et al., 2018). If a solar distance dependent resurfacing process is the cause of the low spectral slopes at low perihelion, it could suggest that the YORP effect could be resurfacing asteroids more often than only at the fission spin rate, as assumed in Graves et al. (2018). It could also mean that another process, such as impacts followed by seismic shaking, may be the dominant process for resurfacing asteroids at small sizes.

The acceptable values of k can provide additional insight. In our model, the timescale of resurfacing scales as $\tau_R \propto r^k$ with $k > 5$, and the best solutions found at lower values of k. This constraint is not surprising, as k needs to be larger than 2 to overcome the increase in the rate of space weathering with decreasing perihelion, which is controlled by the amount of solar insulation. To consider how k compares with the process of thermally induced degradation and with previous studies, it is useful to estimate the dependence of the thermally induced resurfacing timescale from our model on the induced thermal stress. From the arguments in Section 5.1, we assume that the resurface timescale goes as a power law with both thermal stress and solar distance. Furthermore, Molaro et al. (2017) give the relationship between induced thermal stress and solar distance: $\Delta\sigma_s \propto r^{-1.71}$. Thus, using $\tau_R \propto r^k$, we find

$$\tau_R \propto \Delta\sigma_s^m = \Delta\sigma_s^{k/-1.71} \tag{6}$$

where $m \lesssim -3$ to match the range of acceptable solutions in our model, and the best fit solutions are around $m \approx -4.7$.

One approach that has been used in the literature to estimate thermally induced degradation rates is to measure the rate of crack growth for a given boulder size and initial crack length based on induced stress. Migliazza et al. (2011) estimated the dependence of the rate of stable crack growth in a block of marble on the amplitude of induced thermal stress using the Paris law (Paris and Erdogan, 1963): $da/dN \propto \Delta\sigma_s^{3.84}$, where a is the crack length and N is the number of thermal cycles. Delbo et al. (2014) used this result, along with experimental measurements of thermally induced crack growth through meteorites in dry air, to estimate the rate of regolith production on asteroid surfaces. Our parameter would be consistent with that from Migliazza et al. (2011), if we were to assume that the rate of crack growth of a single macroscopic crack is inversely proportional to the resurfacing timescale of an asteroid ($da/dN \propto 1/\tau_R$). However, there are a number of critical issues with making this assumption, which are discussed extensively in Section 4 of Molaro et al. (2017). For one, the results from Migliazza et al. (2011) and Delbo et al. (2014) only quantify the stable regime of crack growth, neglecting the time it takes to form and grow a microcrack into a macroscopic feature. While thermal fatigue can take advantage of preexisting macrocracks emplaced in rocks by impacts and other processes, the growth of new fatigue microcracks driven by mineral heterogeneity will occur simultaneously and eventually dominate the holistic and continuous resurfacing of asteroids at low perihelia. The timescale to grow a microcrack into a macroscopic feature can be orders of magnitude longer than that of stable crack growth (Janssen et al., 2002), suggesting that these models underestimate the total lifetime of objects undergoing breakdown, and thus would not produce the same scaling law as our resurfacing rate. Most importantly, thermally induced breakdown occurs over a range of geomorphic scales, and thus a thermally induced resurfacing rate should reflect the convolved effect of the thermally induced changes to the landscape as a whole. Since da/dN is crack-size

and block-size dependent, the behavior it describes is not representative of such a complex geomorphological process. Ultimately, we argue that the scaling law inferred from our analysis describes something different than the Paris law.

A given value of τ_{R0} is difficult to translate into a timescale of a physical alteration of the surface of an asteroid because τ_{R0} only considers the spectrum of the entire asteroid. However, the rate of regolith production due to thermally induced surface degradation may be closely related. Recent studies of the properties of regolith particles returned from (25143) Itokawa by the JAXA Hayabusa spacecraft have attempted to predict the primary formation process of regolith on Itokawa. Michikami et al. (2018) argued that the axial ratio and shape distribution of the regolith fragments are consistent with being the products of impact fragments and not thermal fatigue. However, Hazeli et al. (2018) argued that the well-rounded profiles and surface textures of the regolith fragments are inconsistent with mechanical fracturing from impact and consistent with thermal fatigue.

Unfortunately, our range of acceptable results cannot help determine which mechanism of regolith production is the most dominant on Itokawa. Depending on the value of τ_{R0}, the thermal breakdown rate at Itokawa's perihelion of about 1 AU could create more or much less regolith compared to that generated by impacts. If a consensus on the presence or production rate of regolith on the surface of Itokawa is reached, we could place a direct constraint on τ_{R0} and greatly shrink the parameter space of acceptable values for τ_{SW0} and k that would be necessary for thermally induced surface degradation to create the spectral slope vs. perihelion trend at $q \lesssim 0.9$ AU. Additionally, two spacecraft missions, OSIRIS-REx and Hyabusa2, are expected to return more regolith samples to Earth in the next five years. Even though these asteroids have different mineralogies than S and Q-type asteroids, studies of their regolith may provide important insights on the presence and rate thermal breakdown on the surface of asteroids.

There are also separate observations and modeling results suggesting that thermal processes can drastically affect asteroids at low perihelia. The asteroid (3200) Phaethon has a perihelion of 0.14 AU, and has experienced unexpected brightening during multiple perihelion passages (Jewitt and Li, 2010; Li and Jewitt, 2013). The brightening is associated with an impulsive release of dust particles near its perihelion (Jewitt and Li, 2010). Due to the high temperatures reached on Phaethon's surface, near surface water ice is not expected to survive. Thus, the most plausible explanation is that thermal fracture of the surface creates dust which is then removed by either the residual velocities of crack growth or through radiation pressure sweeping (Jewitt, 2012).

Additionally, there is evidence that asteroids are completely disrupted at very low perihelia. The model of Granvik et al. (2016) was able to match the distribution of NEAs by instantaneously removing any asteroids from the simulation if they fell below a threshold perihelion, $q \sim 0.05$–0.2 AU. They did not directly model the disruption process, but did suggest 3 possible mechanisms: (1) thermal cracking and removal of grains from radiation pressure, (2) the spin up of asteroids to the point of disruption from the YORP effect (or a similar sublimation driven YORP effect; see Steckloff and Jacobson, 2016), and (3) the sublimation of volatiles present inside the asteroid causing it to blow apart. If thermally induced surface cracking or degradation and the removal of grains from radiation pressure is the primary cause of asteroid resurfacing and disruption at low perihelia, it paints the picture that thermal processes first disrupt the surface of asteroids at a perihelion of $q \lesssim 0.9$ AU. Once the asteroid reaches a perihelion of $q \sim 0.05$–0.2 AU, thermal fracture becomes a runaway process and quickly disrupts the entire asteroid.

As suggested by Jewitt (2012) and Granvik et al. (2016), the removal of dust via radiation pressure sweeping may play an important role in resurfacing and disrupting asteroids. Lofted particles can only be pushed away from an asteroid when the acceleration due to radiation pressure becomes larger than the acceleration due to the gravity of the asteroid. If the residual velocities from thermally induced surface cracking lofts particles off the surface of the asteroid, radiation pressure may push sufficiently small particles away from the asteroid (Jewitt, 2012). We note that simple dust removal (i.e., without any surface degradation) would not be sufficient to give a small asteroid an unweathered spectrum because the surfaces of boulders can be weathered just as effectively as loose material (e.g., Ishiguro et al., 2007). Thus, for an asteroid to have a completely unweathered spectrum, the surfaces of boulders on the asteroid would need to be disrupted to expose unweathered material.

Conversely, surface degradation, followed by overturn or mass movement, without any dust removal, could resurface an asteroid, but it would naturally be a self-limiting process. The fast resurfacing timescale, $\tau_{R0} \approx 150$ kyr, of our best fit solution, shown in Fig. 5, would suggest that the surfaces of asteroids at the Earth's orbit are broken down much more rapidly than the lifetime of NEAs ($\sim$ 10 Myr; Gladman, 2000). Other acceptable solutions permit significantly higher values of τ_{R0}, but asteroids with lower perihelia would still experience surface degradation on a much faster timescale than their lifetimes. If the resulting surface degradation does not remove material from the asteroid, then a thick regolith layer would form and shut off further thermally induced resurfacing. The timescale to create a thick, thermally insulating layer of regolith may also be very dependent on the structure of the surface. Asteroids covered with many boulders may be able to sustain more regolith creation, as material that is disaggregated from the surface of these boulders would fall to the ground below, increasing the time for the entirety of the asteroid to become buried. However, for a very rapid rate of thermal breakdown, some dust removal processes will most likely be required. Fortunately, studies support that this process is reasonable (e.g., Jewitt, 2012; Granvik et al., 2016).

If the weathered material is being removed from the surface in large amounts, we would expect to see a brightening of the asteroid shortly after the dust is released (Jewitt et al., 2015). However, no S or Q-type asteroids with low perihelia have been seen to show any cometary features (Jewitt, 2013). These observations suggest that (1) the removal of surface material is an ongoing process that is occurring very slowly ($\lesssim 1$ kg s^{-1}; Jewitt, 2013), (2) the removal of material happens only periodically and wasn't observed, or (3) the asteroids are somehow being resurfaced without the removal of surface material. It is puzzling that asteroids appear to be completely disrupted at low perihelion (Granvik et al., 2016), but we have only seen evidence of one asteroid (3200 Phaethon) losing mass in that region (Jewitt et al., 2015).

From the above arguments, we cannot conclusively show that thermally induced surface degradation contributed to resurfacing asteroids at low perihelia. However, it is consistent with observations and our basic understanding of thermal fracture. Additionally, other resurfacing processes that could occur at low perihelia cannot explain the rapid change in resurfacing rates that is needed to match the observed spectral slope vs. perihelion distribution. YORP driven spin-up and failure has been cited as a possibility for resurfacing and disrupting asteroids at low perihelion (Nesvorný et al., 2010; Granvik et al., 2016). However, if space weathering is dominated by the solar wind, both the rate of spin-up and failure from the YORP effect (or a sublimation driven YORP effect) and the space weathering rate should identically scale with the amount of solar insolation (see e.g., Graves et al., 2018), resulting in no orbital dependence on the spectral slopes of asteroids.

Granvik et al. (2016) also suggested that the sublimation of volatiles inside asteroids could cause them to blow apart. It could be possible that a similar sublimation of volatiles in the near surface could be breaking apart the surface of S and Q-type asteroids at a slightly higher perihelia than where these asteroids are disrupted. However, S and Q-type asteroids likely experienced heating to 600–960 °C when formed (Keil, 2000), most likely removing the majority of water content from the entire body and making a sublimation driven resurfacing process unlikely.

6.3. Testable predictions of thermally induced surface degradation

In the previous subsection, we discussed how the process of thermally induced surface degradation is a viable mechanism for resurfacing asteroids at low perihelia. Here, we list a few testable predictions from our model:

1. The primary testable result from this study is that the timescale of thermal degradation must scale relatively strongly with solar distance and induced thermal stress. We estimate that the timescale of thermal degradation scales by r^k where $k > 5$, and by $\Delta\sigma_s^m$ where $m < -3$, with the best fit solutions around $k \approx 8$ and $m \approx -4.7$. The value of m could be potentially measured through experimental studies of thermally induced surface degradation with a focus on the entire breakdown process, from crack initiation to failure and disaggregation. These experiments would also need to consider the nature of the breakdown in a vacuum and in objects of different sizes. Finally, the changes in the bulk spectral measurements due to breakdown would need to be measured.
2. S and Q-type asteroids at low perihelion may have high thermal inertia (potentially higher than those with perihelia above $\approx$ 0.9 AU) suggesting that they have lost loose material, or that they are blocky enough to allow significant thermal stresses to build up.
3. If asteroids are resurfaced through thermal effects causing the removal of material, evidence for dust lofting off these asteroids may be observable – even though it was not seen in Jewitt (2013). In particular, Q-types and S-types with low spectral slopes at very low perihelia would be good candidates for observations. However, the resurfacing and removal process needed to change the spectral properties of these asteroids does not require large amounts of material loss, and may be difficult to be observed except in extreme cases (e.g., a total disruption like in Granvik et al., 2016).
4. Thermally induced degradation should be most effective where there is a large temperature change. If resurfacing is connected to thermal effects, then it should be focused in the equatorial regions of asteroids with obliquities near 0° or 180°. If observational geometries allow for an observation biased towards the polar region of one of these asteroids, our model would predict that the asteroid's spectrum would appear more weathered and have a higher spectral slope.
5. Finally, we expect any regolith that is present on asteroids with low perihelia ($q \lesssim 0.9$ AU) to be predominantly created by thermally induced degradation. Whether that regolith will look similar to the regolith on Itokawa is unclear (Michikami et al., 2018; Hazeli et al., 2018), but asteroids at a lower perihelia would have a more pronounced effect.

7. Conclusion

The spectral slopes of S and Q-type asteroids are a strong indicator of the amount of space weathering that has accumulated on their surfaces. Asteroids with lower spectral slopes have most likely been resurfaced recently, and the distribution of these low slopes gives us a powerful constraint to determine which potential resurfacing processes are the most dominant. There are two primary trends in the distribution of spectral slopes: (1) a decrease in spectral slope with decreasing perihelion, and (2) a decrease in the spectral slope with decreasing size. In this study, we tested whether close encounters with the terrestrial planets or thermally induced surface degradation could match the observed spectral slope vs. perihelion distribution. We limited our investigation to only the spectral slope vs. perihelion trend, as the trends are most likely created by different resurfacing processes, and the spectral slope vs. size trend has been previously used as a constraint in Graves et al. (2018).

We found that resurfacing from close encounters could not reproduce the observed spectral slope vs. perihelion distribution for any reasonable combination of parameters. We also argued that previous results supporting close encounters as a viable resurfacing mechanism were due to confounding variables, as the correlation of Q-type asteroids' past orbits with the terrestrial planets are confounded by the higher fraction of Q-type asteroids at low perihelia, most likely created by another resurfacing mechanism.

We found that resurfacing from thermally induced degradation could accurately recreate the observed spectral slope vs. perihelion distribution. We found acceptable solutions with a space weathering timescale for a circular orbit at 1 AU of $\tau_{SW0} \lesssim 5$ Myr, a ratio of the resurfacing timescale to the space weathering timescale of $\tau_{R0}/\tau_{SW0} \gtrsim 2$, and a power law exponent controlling how strongly the resurfacing rate scales with solar distance of $k \gtrsim 5$.

Our acceptable solutions for the power law scaling factor are broadly consistent with the process of thermally induced surface degradation and thermal fatigue. Additionally, other evidence, such as the unexpected brightening of asteroid (3200) Phaethon during its low perihelion passages (Jewitt, 2012) and the complete disruption of asteroids at very low perihelia (Granvik et al., 2016), can also be explained by thermally induced degradation followed by the removal of grains. While more work needs to be done to better constrain the process of thermal breakdown on the surface of asteroids, our work, and specifically Fig. 4, builds a functional relationship between the timescales of space weathering and thermally induced degradation, and the scaling law of thermal degradation which are required to resurface asteroids from thermal effects.

Acknowledgments

K. Graves thanks the NASA Earth and Space Science Fellowship (grant number 17-PLANET17R-0016) for funding. We thank Richard Binzel for a very helpful discussion. We also thank Simone Marchi and Mikael Granvik for their reviews which helped us improve the paper.

References

Auger, A.-T., Groussin, O., Jorda, L., El-Maarry, M.R., Bouley, S., Séjourné, A., Gaskell, R., Capanna, C., Davidsson, B., Marchi, S., Höfner, S., Lamy, P.L., Sierks, H., Barbieri, C., Rodrigo, R., Koschny, D., Rickman, H., Keller, H.U., Agarwal, J., A'Hearn, M.F., Barucci, M.A., Bertaux, J.-L., Bertini, I., Cremonese, G., Da Deppo, V., Debei, S., De Cecco, M., Fornasier, S., Fulle, M., Gutiérrez, P.J., Güttler, C., Hviid, S., Ip, W.-H., Knollenberg, J., Kramm, J.-R., Kührt, E., Küppers, M., Lara, L.M., Lazzarin, M., Lopez Moreno, J.J., Marzari, F., Massironi, M., Michalik, H., Naletto, G., Oklay, N., Pommerol, A., Sabau, L., Thomas, N., Tubiana, C., Vincent, J.-B., Wenzel, K.-P., 2018. Meter-scale thermal contraction crack polygons on the nucleus of comet 67P/Churyumov-Gerasimenko. Icarus 301, 173–188.

Binzel, R.P., Morbidelli, A., Merouane, S., DeMeo, F.E., Birlan, M., Vernazza, P., Thomas, C.A., Rivkin, A.S., Bus, S.J., Tokunaga, A.T., 2010. Earth encounters as the origin of fresh surfaces on near-Earth asteroids. Nature 463, 331–334. https://doi.org/10.1038/nature08709.

Binzel, R.P., Rivkin, A.S., Stuart, J.S., Harris, A.W., Bus, S.J., Burbine, T.H., 2004. Observed spectral properties of near-Earth objects: results for population distribution, source regions, and space weathering processes. Icarus 170 (2), 259–294.

Bottke, W.F., Morbidelli, A., Jedicke, R., Petit, J.-M., Levison, H.F., Michel, P., Metcalfe, T.S., 2002. Debiased orbital and absolute magnitude distribution of the near-Earth objects. Icarus 156, 399–433.

Bottke, W.F., Vokrouhlický, D., Rubincam, D.P., Nesvorný, D., 2006. The Yarkovsky and YORP: implications for asteroid dynamics. Annu. Rev. Earth Planet. Sci. 34 (1), 157–191.

Brunetto, R., Loeffler, M.J., Nesvorný, D., Sasaki, S., Strazzulla, G., 2015. Asteroid Surface Alteration by Space Weathering Processes. Asteroids IV. pp. 597–616.

Brunetto, R., Romano, F., Blanco, A., Fonti, S., Martino, M., Orofino, V., Verrienti, C., 2006a. Space weathering of silicates simulated by nanosecond pulse UV excimer laser. Icarus 180 (2), 546–554.

Brunetto, R., Strazzulla, G., 2005. Elastic collisions in ion irradiation experiments: a mechanism for space weathering of silicates. Icarus 179 (1), 265–273.

Brunetto, R., Vernazza, P., Marchi, S., Birlan, M., Fulchignoni, M., Orofino, V., Strazzulla, G., 2006b. Modeling asteroid surfaces from observations and irradiation experiments: the case of 832 Karin. Icarus 184 (2), 327–337.

Bus, S.J., 1999. Compositional Structure in the Asteroid Belt: Results of a Spectroscopic Survey. PhD thesis. Massachusetts Institute of Technology, Cambridge, MA.

Carry, B., Solano, E., Eggl, S., DeMeo, F., 2016. Spectral properties of near-Earth and Mars-crossing asteroids using Sloan photometry. Icarus (00191035) 268, 340–354. https://doi.org/10.1016/j.icarus.2015.12.047.

Chapman, C.R., 2004. Space weathering of asteroid surfaces. Annu. Rev. Earth Planet. Sci.

32 (1), 539–567.
Clark, B.E., Hapke, B., Pieters, C., Britt, D., 2002. Asteroid Space Weathering and Regolith Evolution. Asteroids III. pp. 585–599.
Delbo, M., Libourel, G., Wilkerson, J., Murdoch, N., Michel, P., Ramesh, K.T., Ganino, C., Verati, C., Marchi, S., 2014. Thermal fatigue as the origin of regolith on small asteroids. Nature 508 (7495), 233–236.
DeMeo, F., Carry, B., 2013. The taxonomic distribution of asteroids from multi-filter all-sky photometric surveys. Icarus 226 (1), 723–741.
DeMeo, F.E., Binzel, R.P., Lockhart, M., 2014. Mars encounters cause fresh surfaces on some near-Earth asteroids. Icarus 227, 112–122.
DeMeo, F.E., Binzel, R.P., Slivan, S.M., Bus, S.J., 2009. An extension of the Bus asteroid taxonomy into the near-infrared. Icarus 202 (1), 160–180.
Dombard, A.J., Barnouin, O.S., Prockter, L.M., Thomas, P.C., 2010. Boulders and ponds on the asteroid 433 Eros. Icarus 210 (2), 713–721.
Eppes, M.C., Magi, B., Hallet, B., Delmelle, E., Mackenzie-Helnwein, P., Warren, K., Swami, S., 2016. Deciphering the role of solar-induced thermal stresses in rock weathering. Geol. Soc. Am. Bull. 128 (9-10), 1315–1338.
Gaffey, M., 1993. Mineralogical variations within the S-type asteroid class. Icarus 106 (2), 573–602.
Gaffey, M.J., 1976. Spectral reflectance characteristics of the meteorite classes. J. Geophys. Res. 81, 905–920.
Gladman, B., 2000. The near-Earth object population. Icarus 146 (1), 176–189.
Granvik, M., Morbidelli, A., Jedicke, R., Bolin, B., Bottke, W.F., Beshore, E., Vokrouhlický, D., Delbò, M., Michel, P., 2016. Super-catastrophic disruption of asteroids at small perihelion distances. Nature 530 (7590), 303–306.
Granvik, M., Morbidelli, A., Jedicke, R., Bolin, B., Bottke, W.F., Beshore, E., Vokrouhlický, D., Nesvorný, D., Michel, P., 2018. Debiased orbit and absolute-magnitude distributions for near-Earth objects. Icarus 312, 181–207.
Graves, K.J., Minton, D.A., Hirabayashi, M., DeMeo, F.E., Carry, B., 2018. Resurfacing asteroids from YORP spin-up and failure. Icarus 304, 162–171.
Hapke, B., 2001. Space weathering from Mercury to the asteroid belt. J. Geophys. Res. 106, 10039–10074.
Hazeli, K., El Mir, C., Papanikolaou, S., Delbo, M., Ramesh, K.T., 2018. The origins of asteroidal rock disaggregation: interplay of thermal fatigue and microstructure. Icarus 304, 172–182.
Hirabayashi, M., 2015. Failure modes and conditions of a cohesive, spherical body due to YORP spin-up. Mon. Not. R. Astron. Soc. 454 (2), 2249–2257.
Ishiguro, M., Hiroi, T., Tholen, D.J., Sasaki, S., Ueda, Y., Nimura, T., Abe, M., Clark, B.E., Yamamoto, A., Yoshida, F., Nakamura, R., Hirata, N., Miyamoto, H., Yokota, Y., Hashimoto, T., Kubota, T., Nakamura, A.M., Gaskell, R.W., Saito, J., 2007. Global mapping of the degree of space weathering on asteroid 25143 Itokawa by Hayabusa/AMICA observations. Meteorit. Planet. Sci. 42 (10), 1791–1800.
Janssen, M., Zuidema, J., Wanhill, R.J.H., 2002. Fracture Mechanics. Delft University Press.
Jewitt, D., 2012. The active asteroids. Astron. J. 143, 66.
Jewitt, D., 2013, May, May. Properties of near-Sun asteroids. Astron. J. 145, 133.
Jewitt, D., Hsieh, H., Agarwal, J., 2015. The Active Asteroids. Asteroids IV. pp. 221–241.
Jewitt, D., Li, J., 2010. Activity in Geminid Parent (3200) Phaethon. Astron. J. 140, 1519–1527 Nov.
Keil, K., 2000. Thermal alteration of asteroids: evidence from meteorites. Planet. Space Sci. 48, 887–903.
Lazzarin, M., Marchi, S., Barucci, M., Di Martino, M., Barbieri, C., 2004. Visible and near-infrared spectroscopic investigation of near-Earth objects at ESO: first results. Icarus 169 (2), 373–384.
Lazzarin, M., Marchi, S., Magrin, S., Licandro, J., 2005. Spectroscopic investigation of near-Earth objects at Telescopio Nazionale Galileo. Mon. Not. R. Astron. Soc. 359 (4), 1575–1582.
Le, J., Manning, J., Labuz, J.F., 2014. Scaling of fatigue crack growth in rock. Int. J. Rock Mech. Min. Sci. 72, 71–79.
Levison, H.F., Duncan, M.J., 1994. The long-term dynamical behavior of short-period comets. Icarus 108, 18–36.
Li, J., Jewitt, D., 2013. Recurrent perihelion activity in (3200) Phaethon. The Astronomical Journal 145, 154 Jun.
Loeffler, M.J., Dukes, C.A., Baragiola, R.A., 2009. Irradiation of olivine by 4 keV He +: simulation of space weathering by the solar wind. J. Geophys. Res. 114 (E3).
Marchi, S., Delbo, M., Morbidelli, A., Paolicchi, P., Lazzarin, M., 2009. Heating of near-Earth objects and meteoroids due to close approaches to the Sun. Mon. Not. R. Astron. Soc. 400, 147–153.
Marchi, S., Magrin, S., Nesvorny, D., Paolicchi, P., Lazzarin, M., 2006a. A spectral slope versus perihelion distance correlation for planet-crossing asteroids. Mon. Not. R. Astron. Soc. Lett. 368 (1), L39–L42.
Marchi, S., Paolicchi, P., Lazzarin, M., Magrin, S., 2006b. A general spectral slope-exposure relation for S-type main belt and near-Earth asteroids. Astron. J. 131 (2), 1138–1141.
Marchi, S., Paolicchi, P., Richardson, D.C., 2012. Collisional evolution and reddening of asteroid surfaces — I. The problem of conflicting time-scales and the role of size-dependent effects. Mon. Not. R. Astron. Soc. 421 (1).
Michikami, T., Kadokawa, T., Tsuchiyama, A., Hagermann, A., Nakano, T., Uesugi, K., Hasegawa, S., 2018. Influence of petrographic textures on the shapes of impact experiment fine fragments measuring several tens of microns: comparison with Itokawa regolith particles. Icarus 302, 109–125.
Migliazza, M., Ferrero, A.M., Spagnoli, A., 2011. Experimental investigation on crack propagation in Carrara marble subjected to cyclic loads. Int. J. Rock Mech. Min. Sci. 48 (6), 1038–1044.
Molaro, J.L., Byrne, S., Langer, S.A., 2015. Grain-scale thermoelastic stresses and spatiotemporal temperature gradients on airless bodies, implications for rock breakdown. J. Geophys. Res. Planets 120 (2), 255–277.
Molaro, J.L., Byrne, S., Le, J.-L., 2017. Thermally induced stresses in boulders on airless body surfaces, and implications for rock breakdown. Icarus 294, 247–261.
Morbidelli, A., Gladman, B., 1998. Orbital and temporal distributions of meteorites originating in the asteroid belt. Meteorit. Planet. Sci. 33, 999–1016 Sep.
Mothé-Diniz, T., Jasmin, F.L., Carvano, J.M., Lazzaro, D., Nesvorný, D., Ramirez, a. C., 2010. Re-assessing the ordinary chondrites paradox. Astron. Astrophys. 514, A86.
Nesvorný, D., Bottke, W.F., Vokrouhlický, D., Chapman, C.R., Rafkin, S., 2010. Do planetary encounters reset surfaces of near Earth asteroids? Icarus 209 (2), 510–519.
Nesvorný, D., Jedicke, R., Whiteley, R.J., Ivezić, ž., 2005. Evidence for asteroid space weathering from the Sloan Digital Sky Survey. Icarus 173 (1), 132–152.
Noguchi, T., Nakamura, T., Kimura, M., Zolensky, M.E., Tanaka, M., Hashimoto, T., Konno, M., Nakato, A., Ogami, T., Fujimura, A., Abe, M., Yada, T., Mukai, T., Ueno, M., Okada, T., Shirai, K., Ishibashi, Y., Okazaki, R., 2011. Incipient space weathering observed on the surface of Itokawa dust particles. Science 333, 1121.
Paolicchi, P., Marchi, S., Lazzarin, M., Magrin, S., 2009. Collisional timing of asteroids space weathering: a first approach. Planet. Space Sci. 57, 216–220.
Paris, P., Erdogan, F., 1963. A critical analysis of crack propagation laws. J. Basic Eng. 85 (4), 528–533.
Reddy, V., Dunn, T.L., Thomas, C.A., Moskovitz, N.A., Burbine, T.H., 2015. Mineralogy and Surface Composition of Asteroids. Asteroids IV. pp. 43–63.
Richardson, D., 1998. Tidal distortion and disruption of Earth-crossing asteroids. Icarus 134 (1), 47–76.
Richardson, J.E., Melosh, H.J., Greenberg, R.J., O'Brien, D.P., 2005. The global effects of impact-induced seismic activity on fractured asteroid surface morphology. Icarus 179 (2), 325–349.
Ritchie, R., 2005. Incomplete self-similarity and fatigue-crack growth. Int. J. Fract. 132 (3), 197–203.
Rivkin, A.S., Thomas, C.A., Trilling, D.E., Enga, M.-t., Grier, J.A., 2011. Ordinary chondrite-like colors in small Koronis family members. Icarus 211, 1294–1297.
Sasaki, S., Nakamura, K., Hamabe, Y., Kurahashi, E., Hiroi, T., 2001. Production of iron nanoparticles by laser irradiation in a simulation of lunar-like space weathering. Nature 410 (6828), 555–557.
Shestopalov, D., Golubeva, L., Cloutis, E., 2013. Optical maturation of asteroid surfaces. Icarus 225 (1), 781–793.
Steckloff, J.K., Jacobson, S.A., 2016. The formation of striae within cometary dust tails by a sublimation-driven YORP-like effect. Icarus 264, 160–171.
Strazzulla, G., Dotto, E., Binzel, R., Brunetto, R., Barucci, M.A., Blanco, A., Orofino, V., 2005. Spectral alteration of the meteorite Epinal (H5) induced by heavy ion irradiation: a simulation of space weathering effects on near-Earth asteroids. Icarus 174 (1), 31–35.
Thirumalai, K., Demou, S.G., 1970. Effect of reduced pressure on thermal-expansion behavior of rocks and its significance to thermal fragmentation. J. Appl. Phys. 41 (13), 5147–5151.
Thomas, C.A., Rivkin, A.S., Trilling, D.E., Grier, J.A., 2011. Space weathering of small Koronis family members. Icarus 212 (1), 158–166.
Thomas, C.A., Trilling, D.E., Rivkin, A.S., 2012. Space weathering of small Koronis family asteroids in the SDSS Moving Object Catalog. Icarus 219 (1), 505–507.
Vernazza, P., Binzel, R.P., Rossi, A., Fulchignoni, M., Birlan, M., 2009. Solar wind as the origin of rapid reddening of asteroid surfaces. Nature 458 (7241), 993–995.
Viles, H., Ehlmann, B., Wilson, C.F., Cebula, T., Page, M., Bourke, M., 2010. Simulating weathering of basalt on Mars and Earth by thermal cycling. Geophys. Res. Lett. 37, L18201.
Walsh, K.J., Richardson, D.C., 2008. A steady-state model of NEA binaries formed by tidal disruption of gravitational aggregates. Icarus 193 (2), 553–566.
Walsh, K.J., Richardson, D.C., Michel, P., 2008. Rotational breakup as the origin of small binary asteroids. Nature 454, 188–191.
Willman, M., Jedicke, R., Moskovitz, N., Nesvorný, D., Vokrouhlický, D., Mothé-Diniz, T., 2010. Using the youngest asteroid clusters to constrain the space weathering and gardening rate on S-complex asteroids. Icarus 208, 758–772.